Materials Today Bio 16 (2022) 100434

Contents lists available at ScienceDirect

Materials Today Bio

journal homepage: www.journals.elsevier.com/materials-today-bio

Aptamer engineering exosomes loaded on biomimetic periosteum to promote angiogenesis and bone regeneration by targeting injured nerves via JNK3 MAPK pathway

Yanlin Su [a,1], Qing Gao [a,1], Rongli Deng [b,1], Lian Zeng [a], Jingyi Guo [c], Bing Ye [a], Jialin Yu [d], Xiaodong Guo [a,*]

[a] Department of Orthopedics, Union Hospital, Tongji Medical College, Huazhong University of Science and Technology, Wuhan, Hubei 430022, China
[b] PCFM Lab, School of Chemistry and School of Materials Science and Engineering, Sun Yat-sen University, Guangzhou, Guangdong 510000, China
[c] College of Arts and Science of Hubei Normal University, Huangshi, Hubei 430022, China
[d] The First Affiliated Hospital of Yangtze University, Jingzhou, Hubei 430022, China

ARTICLE INFO

Keywords:
Aptamer
Engineering exosomes
Electrospinning
Repaired schwann cells
Nerve regeneration
Bone regeneration

ABSTRACT

Repairing critical bone defects is a complex problem in the clinic. The periosteum rich in nerve plays a vital role in initiating and regulating bone regeneration. However, current studies have paid little attention to repairing nerves in the periosteum to promote bone regeneration. Thus, it is essential to construct bionic periosteum with the targeted injured nerves in the periosteum. We coupled phosphatidylserine (PS) targeted aptamers with repair Schwann cell exosomes to construct exosome@aptamer (EA). Then through PEI, EA was successfully built on the surface of the electrospun fiber, which was PCL@PEI@exosome@aptamer (PPEA). Through SEM, TEM, and other technologies, PPEA was characterized. Experiments prove in vivo and in vitro that it has an excellent repair effect on damaged nerves and regeneration of vascular and bones. In vivo, we confirmed that biomimetic periosteum has an apparent ability to promote nerve and bone regeneration by using Microcomputer tomography, hematoxylin-eosin, Masson, and Immunofluorescence. In vitro, we used Immunofluorescence, Real-Time Quantitative PCR, Alkaline phosphatase staining, and other tests to confirm that it has central nerve, blood vessel, and bone regeneration ability. The PPEA biomimetic periosteum has apparent neurogenic, angiogenic, and osteogenic effects. The PPEA biomimetic periosteum will provide a promising method for treating bone defects.

1. Introduction

The critical bone defect is a complicated problem in clinical practice, which causes a severe economic burden to patients and society. Many materials with osteogenic ability have been used to induce bone regeneration and even osteoporotic bone regeneration [1–4].

The periosteum plays a significant role in the developmental process of the bone in the physiological state and the repair process in the pathological condition by storing progenitor cells and serves as a source of local growth factors and a scaffold for the recruitment of cells and other growth factors [5]. Loss of osteogenic-associated cells and osteogenic-induced signals due to inactivation and removal of the periosteum is a fundamental reason for the poor healing of allogeneic bone grafts [6]. In recent years, the repair of the periosteum has attracted more and more attention as an indispensable part of the bone tissue repair process. However, Autologous osteochondral grafts have limited sources and are prone to deep tissue infection and chronic pain at the harvest site [7]. Allogeneic osteochondral grafts may also lead to immune reactions and pathogen transmission [8]. Therefore, building an artificial biomimetic periosteum with structural and functional similarity to natural periosteum is an effective bone tissue treatment.

The natural periosteum contains large neural networks, which is very important for the periosteum to promote bone regeneration. Recent studies revealed that sensory nerves are essential for initiating and regulating vascular and bone regeneration [7–11]. Tomlinson confirmed that NGF is a skeletal neurotrophin to promote sensory innervation of developing long bones, a process critical for normal primary and secondary ossification [9]. Hu demonstrated that the PGE2/EP4 axis in the

* Corresponding author.
E-mail address: xiaodongguo@hust.edu.cn (X. Guo).
[1] These authors contributed equally.

https://doi.org/10.1016/j.mtbio.2022.100434
Received 5 August 2022; Received in revised form 12 September 2022; Accepted 14 September 2022
Available online 20 September 2022

sensory nerve could participate in bone regeneration by regulating MSCs differentiation in the bone marrow of mice [10]. Li discovered that calcitonin gene-related peptide (CGRP) secreted by sensory nerves could promote bone regeneration, confirming that nerves play an unnoticeable role in bone tissue healing [11]. Therefore, inducing nerve regeneration in the periosteum provides a new idea to facilitate the repair of bone defects. Although autologous nerve grafting remains the gold standard for peripheral nerve injury, limited sources, repeated surgeries, and impaired function at the harvest site have limited its use [12–14]. With the rapid development of tissue engineering, many synthetic nerve grafts have been used instead of autologous nerve grafts for nerve repair, and grafts have been improved by introducing various cells and neurotrophic factors into the grafts. Biomaterials that are biocompatible because they are inert will lack bioactivity and not provide a suitable microenvironment for nerve regeneration [15]. Therefore, it is crucial to construct a biocompatible and biologically active pro-neural regeneration biomimetic membrane to repair injured nerves. Angiogenesis plays an essential role in bone regeneration. Some studies have shown that mesenchymal stem cells overexpressing Wnt10a can promote skull repair through VEGF-mediated angiogenesis [16].

Studies showed that exosomes in the nervous system contain miRNAs that regulate regeneration, with exosomes from Schwann cells promoting peripheral nerve regeneration [17]. Exosomes are extracellular vesicles secreted by cells and contain complex RNAs and proteins. As the key players of intercellular communication, exosomes play a fundamental role in the physiological and pathological processes of the nervous system [18,19]. Accumulating evidence has suggested that exosomes can treat nerves by mediating axonal regeneration, activating Schwann cells, promoting vascular regeneration, and regulating inflammation [20]. Although the above evidence demonstrates that Schwann cell-derived exosomes have a pro-neural regenerative effect, the limited therapeutic effect is a problem that we must consider. Recent studies have shown that when peripheral nerves are injured, myelin and non-myelin Schwann cells distal to the nerve injury are reprogrammed under the regulation of the transcription factor C-JUN to generate repair Schwann cells (Bungner cells) [21]. Compared to normal Schwann cells, these repairing Schwann cells exhibits powerful functions in guiding and promoting axonal regeneration [22]. Therefore, it is an excellent strategy to construct tissue engineering materials with repair Schwann cell exosomes for the repair process of peripheral nerves.

Many researchers are exploring different directions to solve the low targeting of exosomes. Among them, the engineering method of chemical modification is fundamental. Recent studies have shown that phosphatidylserine (PS) is a lipid in cells exposed to the surface after axonal injury [23]. PS is essential in identifying and promoting axon fusion and regeneration after injury [24]. In this experiment, the PS-aptamer, the aptamer targeting PS, was synthesized [25]. The aptamer was combined with the extracted repair Schwann cell exosomes by self-assembly to construct exosomes with PS targeting, which was Aptamer@Exosome (EA).

Partial absence or deficiency of the microstructure of the raw nerve may cause inhibition of axonal extension or misdirected axonal extension during nerve repair [26]. Numerous studies indicated that fiber-like or channel-like microstructures arranged longitudinally could guide neurite growth during neurite growth [27–30]. Recent studies have found that introducing axially aligned microchannel structures into the bio-scaffold could effectively guide and significantly facilitate neurite extension and Schwann cell migration [31,32]. As a common material for bone tissue engineering, polycaprolactone (PCL) has good biocompatibility, fewer acid decomposition products, good mechanical properties, and a slow degradation rate, providing time for tissue remodeling [33,34]. However, because natural PCL does not have a microstructure similar to the biological extracellular matrix, it cannot provide a suitable microenvironment for tissue regeneration. Fortunately, electrostatic spinning technology has successfully produced electrospun nanofibers with similar structures to the natural extracellular matrix using a range of combinations, including polymers and ceramics as materials [35,36]. Therefore, constructing a biomimetic periosteum with guided microstructure by electrospinning technology using PCL as the material is of great importance for neural and bone regeneration.

This study aimed to construct guided electrospun membranes using PCL and loaded EA through PEI self-assembly; PEI has a large number of amino groups and shows a large number of positive charges [37]. In contrast, electrospun PCL and exosome surfaces both have negative charges and can load exosomes on PCL via electrostatic interactions [38]. Finally, a biomimetic periosteum with exosome activation was synthesized, which was PCL@PEI@Exosome@PS-Aptamer (PPEA). PEI first adsorbs protons from acid at decreasing acid-base, and EA was released from PPEA. Furthermore, in vivo and in vitro experiments will verify the biomimetic periosteum to promote neuroaxonal fusion, vessel regeneration, and bone regeneration. The PPEA biomimetic periosteum will provide a promising therapeutic approach for bone regeneration (see Scheme 1).

2. Method

2.1. Preparation of electrospun biomimetic periosteum

The PCL solution was prepared by dissolving PCL particles (12%w/v) in 2,2,2-trifluoroethanol (TFEA) to prepare the shell solution. To prepare core-shell nanofibers, the answer was simultaneously pumped from a 10 ml syringe through a spinneret (17 G). A PCL solution with a flow rate of ~ one ml/h was used for coaxial electrospinning at 13 kV using a voltage regulator DC power supply (Tonli; Shenzhen, China). The vertically arranged nanofibers are electrospun on a roller, and the distance between the spinneret and the collector is 10 cm. A roller with a diameter of 15 cm and a width of 10 mm is connected to a negative voltage of −1.5 kV and rotates at 3000 rpm. The membranes are placed in 70% ethanol for 3 h to sterilize.

2.2. Construction of PPEA biomimetic periosteum

2.2.1. Extraction and loading of repaired Schwann cell exosomes

2 ng/ml Transforming growth factor-β (TGF-β) was added to the medium for 1 h to stimulate the transformation of Schwann cells into repaired Schwann cell. After the reconstituted Schwann cells were successfully constructed, the cell supernatant was extracted. The sample was moved to a new centrifuge tube, 2000 g, Centrifuge **(**Microfuge 20R, Beckman, Germany**)** at 4 °C for 30 min. Then transfer the supernatant to a new centrifuge tube, 10000 g, Centrifuge, at 4 °C for 45 min to remove more giant vesicles. Remove the supernatant after 0.45 μ M filter membrane and collect the filtrate. Transfer the filtered liquid to a new centrifuge tube, and select the Overspeed rotor, 4 °C, 100000 g centrifugation (CP100MX, Hitachi, Japan) for 70 min. Remove the supernatant with 100 μ L precooled 1 × PBS re suspension, take 20 μ L for the electron microscope, 10 μ L as particle size, 10 μ L-extracted protein was used for Western blot, and the remaining exosomes were stored at −80 °C.

2.2.2. Construction of aptamer engineering exosomes

PS aptamer was synthesized by Accurate Biotechnology (Hunan) Co., Ltd., and its sequence is 5′-AAA GAG-3'. The extracted exosomes with a concentration of 3*10^9/ml were mixed with 4% PEG-COOH at room temperature for 24 h and successfully constructed exosome@PEG-COOH. Exosome@PEG-cooh and PS-aptamer are combined through a condensation reaction. The condensation process is carried out at room temperature, and the EDC activator (D1601, TCI, Japan) is used to catalyze for 24 h. First, prepare PEI solution (5 × 10 ^-3 moL/l) 10 ml, put PCL electrospun film into PEI solution, treat it for 1 h by rotating and stirring, and wash it with distilled water for 5min. Finally, the electrospun periosteum was incubated with exosome extract with a density of 3.99 × 10^4ml-1 for 24 h and, after drying at the critical point, observed by scanning electron microscope.

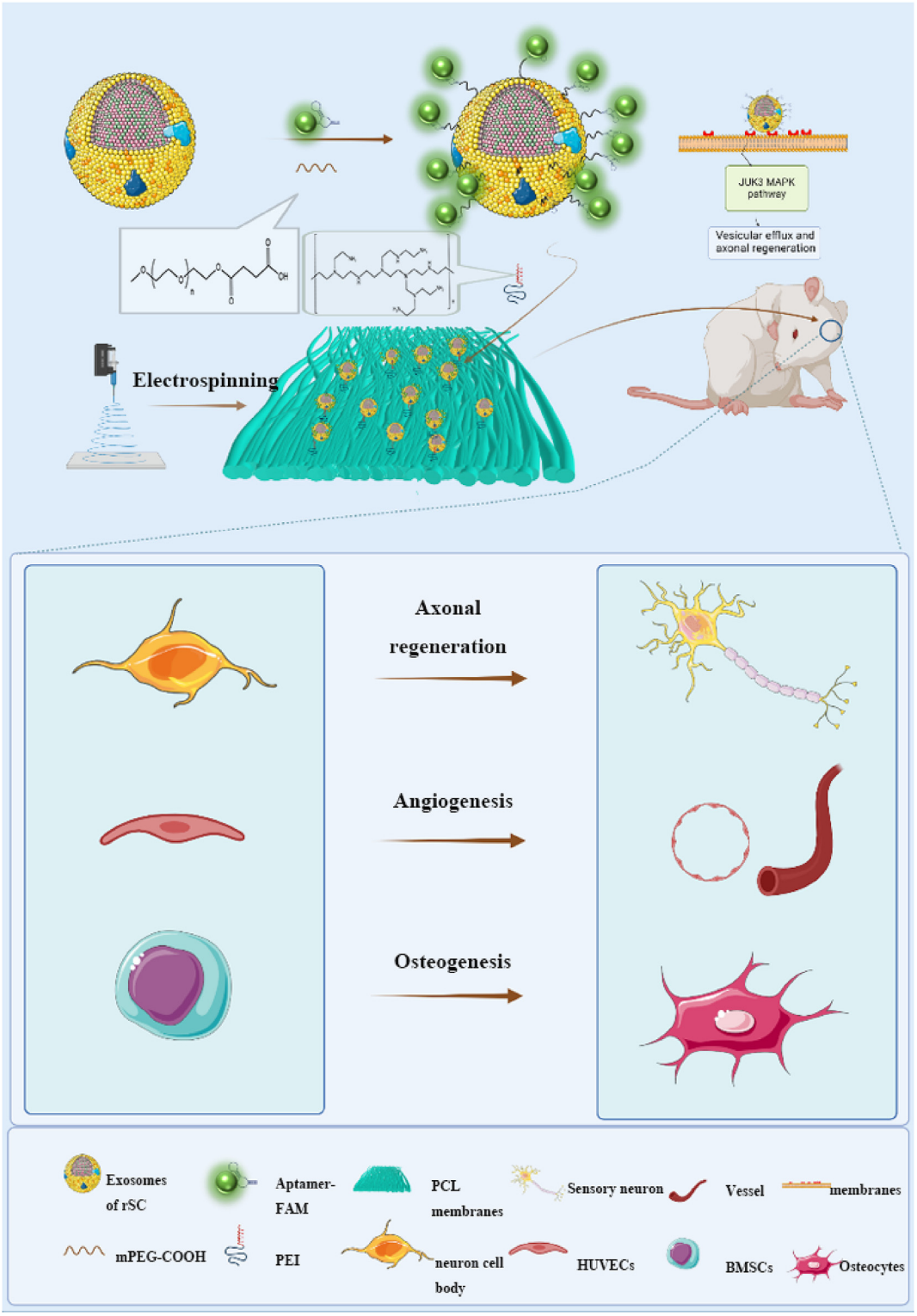

Scheme 1. The schematic diagram shows that PPEA electrospun biomimetic periosteum loaded with aptamers engineered exosomes can target injured axons and regenerate blood vessels and bone.

2.3. Material characterization

After gold sputter-coating of the specimens, the external morphology of the biomimetic periosteum was characterized using scanning electron microscopy (SEM) and described at an operating voltage of 15 kV. The microstructure of the biomimetic bone membrane was characterized by transmission electron microscopy (TEM). The Fast Fourier Transform (FFT) analysis of the biomimetic periosteum was performed using ImageJ. In order to explore the release curve of exosomes in PPEA biomimetic periosteum, the exosomes were washed with PBS for 3 times after 24 h of loading, and then 0.1cm × 0.1 PPEA biomimetic periosteum was soaked in 100 μ L PBS was incubated on a horizontal shaking table at 37 °C and 60 rpm for 14 days. HCl and NaOH were used to adjust the pH of PBS to 6.4, 7.4, and 8.4, respectively, and 80 μ L supernatant and

supplement 80 μ L fresh PBS, use BCA protein detection kit to detect the concentration of exosomes in the supernatant.

2.4. Animals and surgical procedures

All animal experiments were reviewed and approved by the Animal Ethics Committee of Huazhong University of Science and Technology (Animal ethics number: s2755). All animals are fed in a sterile environment according to regular feeding practices. Eighteen 6–8week C57BL/6 (female; 30 g) were randomly divided into three groups: (1) PCL group; (2) PPE group; (3) PPEA group. The cranial defect model was established according to a previous report [39]. After anesthetizing the rats, the rats' head hair was shaved, and a 1.5 cm incision was made. Then, after creating a critical size bone defect of 5 mm in diameter, a periosteum was implanted to fill the bone defect, and the wound was sutured closed. The surgery was performed under aseptic conditions, and postoperative antibiotics were administered to prevent infection. 8 weeks later, the animals were executed, and all skull bones were collected and fixed in a 4% paraformaldehyde solution.

2.5. Cell culture

2.5.1. DRG and sensory neuron extraction

Cells were obtained from 3–5-day SD rats. Briefly, after mice were disinfected, their heads were removed, and the spinal canal was opened. DRG was extracted using microscopic tweezers and cultured in Dulbecco's modified eagle's medium (DMEM; Hyclone Laboratories, USA) containing 10% fetal bovine serum (FBS; Gibco, Thermo Fisher Scientific, USA). Following adherence to the wall, they were cultured in Neurobasal-A Medium (Gibco) + B27 (Gibco). Half of the culture medium was changed the next day and reserved. Sensory neuron cells were digested with 0.25% trypsin for 45 min, centrifuged, resuspended with fresh culture medium, planted in a Petri dish, and set aside.

2.5.2. Schwann cells and HUVECs

The Schwann cell line (RSC96), and human umbilical vein endothelial cells (HUVECs) were purchased from Procell (Wuhan, China). It was cultured in DMEM/F12 basic medium (Hyclone) + 8% FBS (Hyclone) + 1% penicillin/streptomycin (Solarbio, Beijing, China). The medium was changed for three days, and cells were subcultured when they reached 90% confluence.

2.5.3. BMSCs

BMSCs were extracted from the bone marrow. A syringe was used to absorb the precooled PBS to flush out the bone marrow from the femurs of 3–5-day SD rats. Next, a low-temperature centrifuge (Microfuge 20R, Beckman, Germany) was used to centrifuge samples at 1000 rpm for 5 min, following which the supernatant was removed and cultured in DMEM/F12 basic essentialism (Hyclone) + 8% FBS (Hyclone) + 1% penicillin/streptomycin (Solarbio). The medium was changed for 3 days, and cells were subcultured when they reached 90% confluence. BMSCs were identified by immunofluorescence staining of CD29 (Fig. S1).

2.6. Immunofluorescence

Cells or tissue were fixed with PBS containing 4% PFA for 20 min. Cells were blocked and permeabilized with PBS containing 0.2% Triton-100 and 2% fish skin gelatin (Sigma) in a humidified chamber (30 min). Cells were incubated with primary antibodies against C-JUN (ab40766, Abcam, USA), NF200 (ab134306, Abcam, USA), OCN (ab133612, Abcam, USA) overnight at 4 °C and then incubated with fluorescently labeled secondary antibodies (8889S, Cell Signaling Technology, Beverly, MA, USA) for 1 h. After staining with DAPI (ab228549, Abcam, USA) for 5 min and observed with a fluorescent microscope (IX73, Olympus, Tokyo, Japan). Quantitative analysis was performed using ImageJ.

2.7. Western blot analysis

After extraction, the protein samples were separated by polyacrylamide electrophoresis according to molecular weight. After obtaining the desired results, the proteins are transferred to the hybridization membrane. The membrane is closed with a blocking solution and incubated with diluted primary antibody against C-JUN (ab40766, Abcam, USA), β-actin (ab8226, Abcam, USA), Calnexin (ab133615, Abcam, USA), TSG101 (ab125011, Abcam, USA), JNK3 (ab124956, Abcam, USA). And the second antibody for 1 h. Moreover, the detection was performed using a high-sensitivity ECL luminescence instrument (Gene Gnome XRQ NPC, Cambridge, UK). Quantitative analysis was performed using ImageJ.

2.8. Real-time quantitative PCR analysis

Total RNA was extracted in strict accordance with the instructions of Trizol (AG21101, Accurate Biotechnology (Hunan) Co., Ltd., Hunan, China). The primer sequence is in Table S1. PrimeScript Reverse Transcriptase kit (AG11702-S, Accurate Biotechnology (Hunan)Co., Ltd., China) was used to synthesize cDNA. cDNA was quantified using SYBR Green PCR kit (AG11701-S, Accurate Biotechnology (Hunan)Co., Ltd, China) for quantitative analysis. The expression of the genes was calculated by the $2^{-\Delta\Delta t}$ method.

2.9. Axon target assay

DRG cells were cultured in a six-well plate. After the nerve cells mature, Blade cutting axon at about 50 μm in front of the cell body. Then the cells were stained with Nile red. The 50 μl EA was added to the six-well plate. After 30 min, observed with a fluorescence microscope and analyzed with ImageJ.

2.10. Tube formation assay

Basement membrane extract (BME) purchased from BD Biosciences was prepared one day in advance. After adding BME to a 96-well plate to cover the bottom of the wells, HUVECs and culture medium from DRG on biomimetic periosteum were co-cultured on the scale (37 °C, 4 h). After staining with Calcein-AM (ab228556, Abcam, USA), the formation of tubes on the cell plates were observed with a fluorescent microscope (IX73, Olympus, Japan). The vascular network was quantified using ImageJ.

2.11. AR and ALP staining

Cells (1 × 10ˆxu6) were seeded in a complete culture medium, and different components of biomimetic periosteum were added to cultivate the DRG culture medium. After 14 days of culture, cells were fixed with 4% paraformaldehyde and stained with AR (Sigma-Aldrich, St. Louis, MO, USA) and ALP (Sigma-Aldrich, USA). Images were obtained using a fluorescence microscope (IX73, Olympus, Tokyo, Japan). Quantitative analysis was performed using ImageJ.

2.12. Micro-CT

Collected samples were fixed in 4% paraformaldehyde, placed in a polymethylmethacrylate scaffold, and subjected to micro-CT scanning (SkyScan 1176, Bruker). The X-ray beam energy was set to 70 kVp, the intensity was 109 A, and the maximum resolution was 9 μm. After scanning, the obtained 2D slices were stacked into a 3D model. Bone volume, bone mineral density, and the number and thickness of trabeculae in the segmented area were calculated.

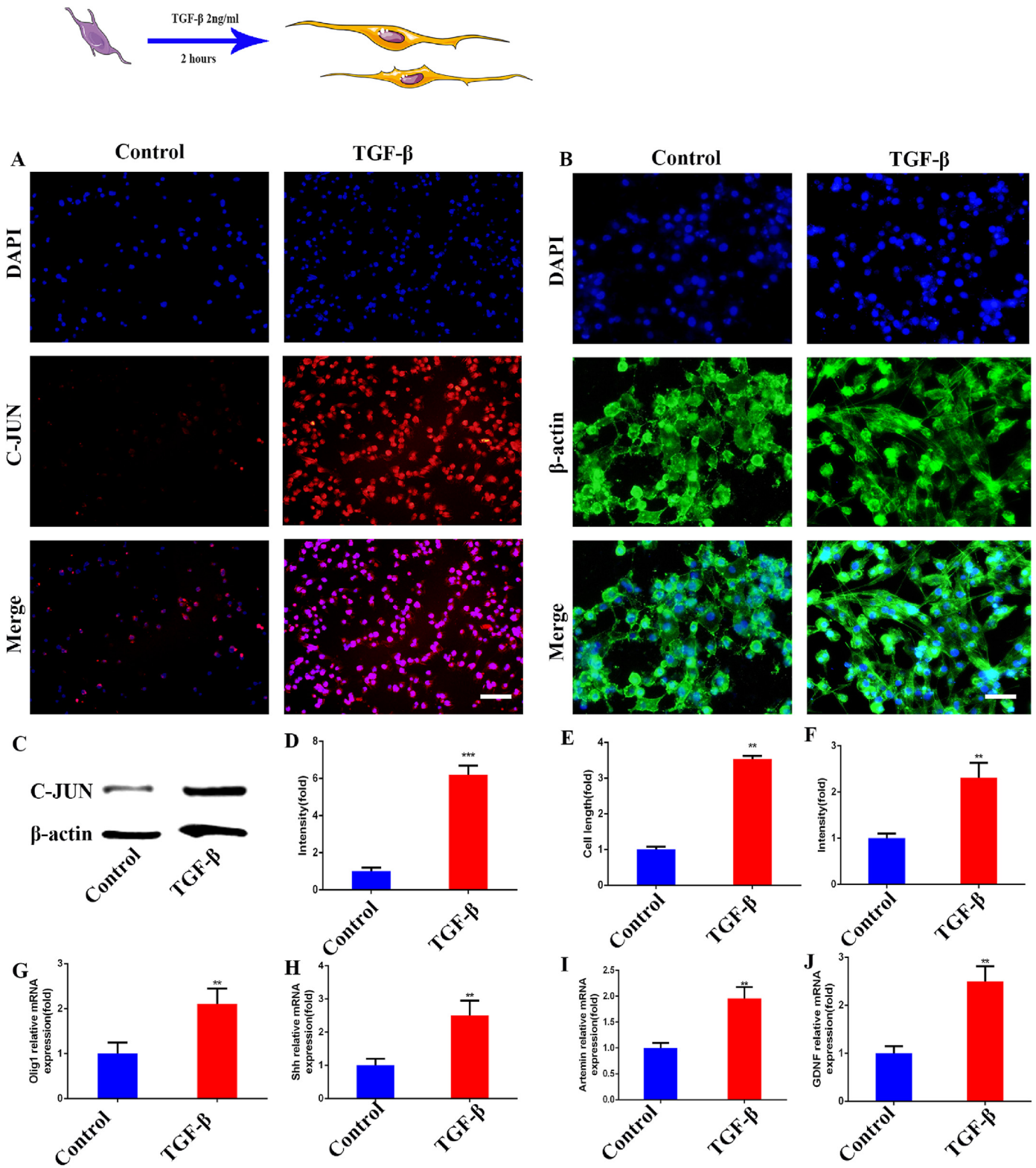

Fig. 1. Construction of repair Schwann cells. (A) Immunofluorescence detection of C-JUN expression in Schwann cells. (B) Immunofluorescence detection of Schwann cell morphology. (C) Western blot detection of the expression of C-JUN in Schwann cells. (D)The quantitative analysis of A. (E)The quantitative analysis of B. (F) The quantitative analysis of C. (G–J) The RT-qPCR detection of the mRNA expression of Olig1, Shh, artemin, and GDNF in Schwann cells. Scale bar = 100 μm in panels (A), 50 μm in panels (B). N = 3,$^{**}p < 0.01$, $^{***}p < 0.001$.

2.13. HE

The harvested specimens were fixed in a 4% paraformaldehyde solution, dehydrated with alcohol, and transparent with a xylene clearing agent. The transparent tissue blocks were embedded in wax, sectioned with a microtome, and attached to slides. The samples were dewaxed and stained with Hematoxylin (H) dye and Eosin (E) dye (ab245880, Abcam, USA). The sections were dehydrated with alcohol and then made

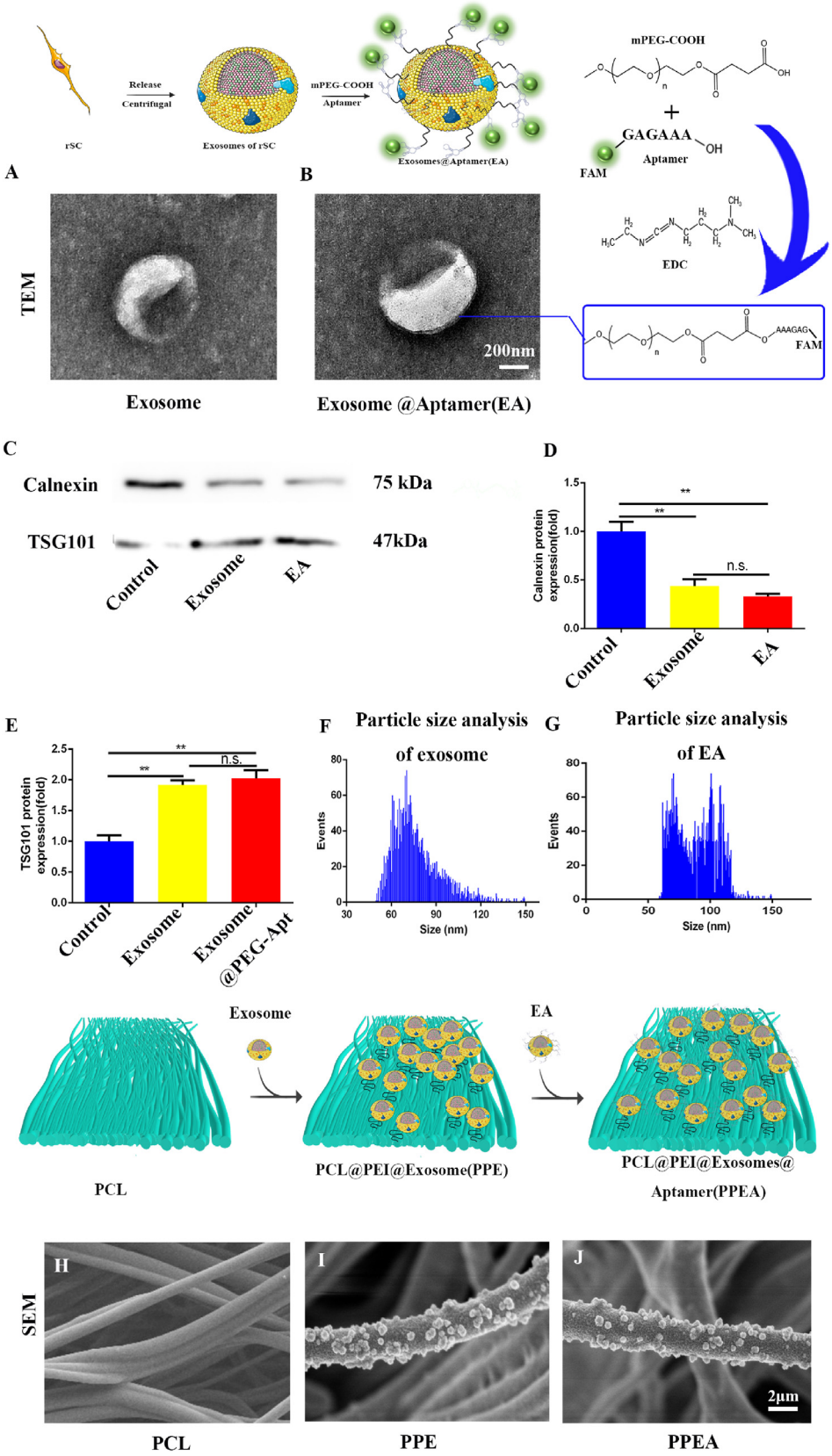

Fig. 2. Exosome identification and construction of exosome activated biomimetic periosteum. (A, B) TEM exosome identification. (C) Detection of exosome markers by Western blot. (D, E) The quantitative analysis of B. (F, G) Particle size analysis of exosomes and EA. (H–J) SEM identification of biomimetic periosteum by electrospinning and biomimetic periosteum loaded with exosomes. Scale bar = 200 nm in panels (A), 2 μm in panels (G, H). N = 3, ***p < 0.001.

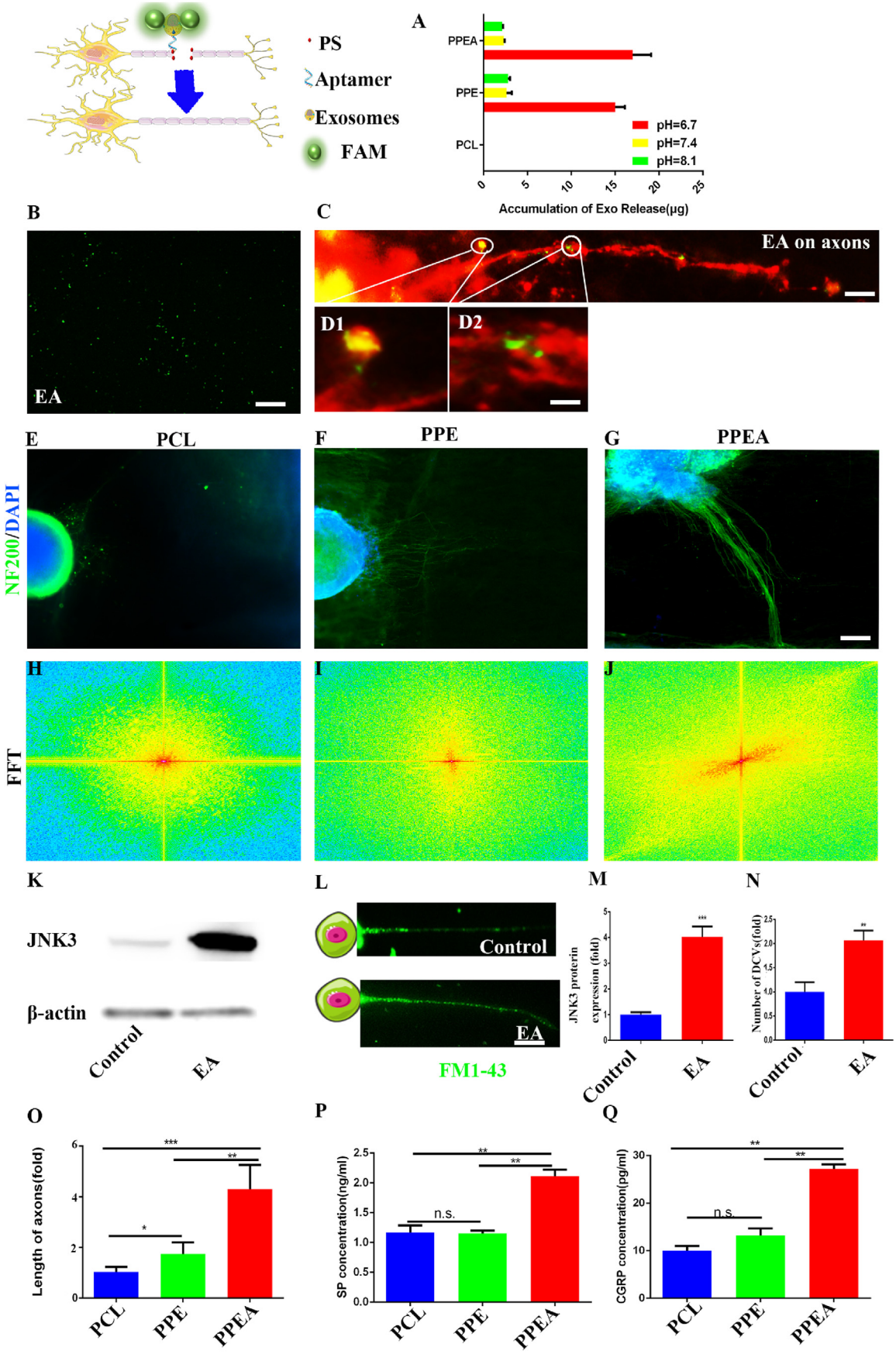

Fig. 3. PPEA biomimetic periosteum releases exosomes to repair nerves and promote axonal regeneration.

transparent with xylene. The cells were sealed and placed under a microscope for observation.

2.14. Masson

Paraffin sections were dewaxed to water and then homogenized. After washing with tap water and distilled water, the nuclei were stained with Regaud hematoxylin staining (GENTA02077, Gentaur Ltd, UK) or Weigert hematoxylin solution (HT1079, Merck, USA) for 5–10 min. After sufficient water washing, the samples were stained with Masson Lixin Red acidic reddish solution for 5–10 min. After washing with 2% glacial acetic acid aqueous solution for a few moments, 1% phosphomolybdic aqueous acid solution was added for 3–5 min, and then directly stained samples with aniline blue or photo green solution for 5 min. The samples were sealed with 95% alcohol, anhydrous alcohol, xylene transparent, and neutral gum. Quantitative analysis of collagen was performed using ImageJ.

2.15. Enzyme-linked immunosorbent assay (ELISA)

After three days of treatment, the cell culture media were changed. After three days of culture, extracellular fluid was extracted and stored in a −80 °C refrigerator. Next, extracellular fluid was removed thrice, centrifuged at 3000 rpm for 20 min, and the supernatant was collected. An ELISA Kit (Dignity biology, Shanghai, China) was used to detect neurotrophic factors, per the manufacturer's instructions. Briefly, standard and sample wells were established, measure, and sample were added to their respective holes, treated with 100 μl of the Horseradish peroxidase (HRP), and incubated at 37 °C for 60 min after sealing the plate. The supernatant was removed and treated with a chromogenic agent, and the absorbance (OD) at 450 nm was analyzed using an enzyme labeling instrument (Multiskan GO, Thermo Fisher Scientific).

2.16. EdU assay

The proliferation of HUVECs was assessed using the BeyoClick™ EdU Cell Proliferation Kit (Beyotime, China). After adding the EdU medium dilution according to the manufacturer's instructions, the culture medium from DRG on biomimetic periosteum was co-cultured with the cell samples for three days. The cells were then washed 1–2 times with PBS, and EdU staining was observed under an inverted fluorescent microscope (IX73, Olympus, Japan). Quantitative analysis was performed using ImageJ.

2.17. Statistical analysis

Means and standard deviations were calculated in groups, and data were presented as mean ± standard deviation (SD). Statistical analysis was performed using one-way ANOVA (GraphPad Software, USA). Tukey's post hoc test analyzed the statistical significance between groups. Values of $P < 0.05$ were considered statistically significant.

3. Results and discussion

3.1. Schwann cells successfully transformed into repair Schwann cells

In recent reports, Schwann cells were reprogrammed and transformed into repair Schwann cells after sciatic nerve injury [40]. C-JUN, Olig1, Shh, artemin, and GDNF were significantly up-regulated. Previous studies showed that TGF- β can up-regulate C-JUN in Schwann cells, and C-JUN played a vital role in the reprogramming of Schwann cells [41]. We used 2 μg/ml TGF- β to stimulate Schwann cells for 2 h and tried to construct a repair Schwann cell model. As shown in (Fig. 1A, D), After TGF- β stimulation, the expression of C-JUN increased significantly, which was 6.19 times that of the control group. At the same time, the length of stimulated cells was detected, and it was found that the size increased significantly, which was 3.54 times that of the control group (Fig. 1B, E). The protein expression of the C-JUN in the cells was also detected. As shown in the figure, the protein expression was significantly increased, which was 2.31 times that of the control group (Fig. 1C, F). To further verify the construction of the repair phenotype, we detected the mRNA expression of several key markers (Olig1, Shh, artemin, GDNF) in the cell repair phenotype. As shown in the figure, Olig1 was 2.11 times as much as that in the control group (Fig. 1G), Shh was 2.51 times as much (Fig. 1H), artemin was 1.96 times as much (Fig. 1I), and GDNF was 2.49 times as much (Fig. 1J), all showing a significant increase. From the above results, we successfully constructed the Schwann cell repair phenotype. Preparation for further extraction of exosomes.

3.2. Construct PPEA electrospun biomimetic periosteum

There will be apparent immune rejection as cells are implanted in the defect site [42]. As messengers carrying the critical substances of cellular miRNA and protein, Exosomes are essential for bone regeneration. Planting exosomes will significantly reduce immune rejection. It is a promising direction to modify the cells that produce exosomes [43].

Therefore, we successfully constructed and repaired Schwann cell exosomes through the previous step. Next, we coupled PS aptamer with exosomes through mPEG-COOH so that exosomes could target PS. As shown in (Fig. 2A and B), transmission electron microscopy showed that exosomes were successfully extracted, and PS aptamers were modified to the surface of exosomes.

Subsequently, we detected the exosome membrane protein. As shown in (Fig. 2C), the expression of exosome marker Calnexin was decreased, and TSG101 was significantly increased. PPEA and PPE were 0.46 and 0.32 times that of the control group in Calnexin. PPEA and PPE were 1.96 and 2.11 times that of the control group in TSG101 (Fig. 2C–E). At the same time, we detected the particle size of the extracted exosomes, and the diameter of the extracted exosomes was between 30 and 150 nm, which was consistent with the exosome diameter (Fig. 2F and G). The above evidence proved that we have successfully extracted the repaired Schwann cell exosomes and successfully modified the surface of exosomes.

Polyethylenimine (PEI) is a widely used coupling agent. Because it has many amino groups, it shows many positive charges, which is very suitable for use as a coupling agent between PCL and exosomes [44]. As shown in the figure, SEM shows that the exosomes are successfully loaded onto electrospun fibers through the electrostatic interaction of positive and negative charges. We constructed biomimetic periosteal scaffolds using PCL as raw material by ordered electrospinning technology (Fig. S2A). SEM showed that electrospinning technology obtained the biomimetic periosteum using PCL as raw material. EA was successfully loaded on biomimetic periosteal fibers (Fig. 2H–J, Fig. S2C). Finally, we successfully constructed the biomimetic periosteum (PPEA). We tested the biocompatibility of the synthetic biomimetic periosteum and co-cultured the biomimetic periosteum with PC12 cells, a neural cell line. As shown in Fig. S3A–I, the biocompatibility of the three kinds of bionic periosteum is quite good without significant differences. We then examined the degradation of the bionic periosteum and the survival time of EA. The bionic periosteum of PPEA was degraded by 52% at 28 days (Fig. S4). The survival time of exosomes on biomimetic periosteum can reach 56 days (Fig. S5).

3.3. Targeting and promoting axon regeneration

Next, we are exploring the release of biomimetic periosteum under different pH conditions. The pH of the microenvironment afthe ter bone defect was about 6.7 [45]. To mimic the acid-base environment in vivo, we placed the biomimetic periosteum in PBS buffer at a pH similar to that in vivo. It can be seen from the figure that after the pH drops to 6.7, the release of exosomes in PPEA increases significantly, which is 7.48 times that PCL group (Fig. 3A).

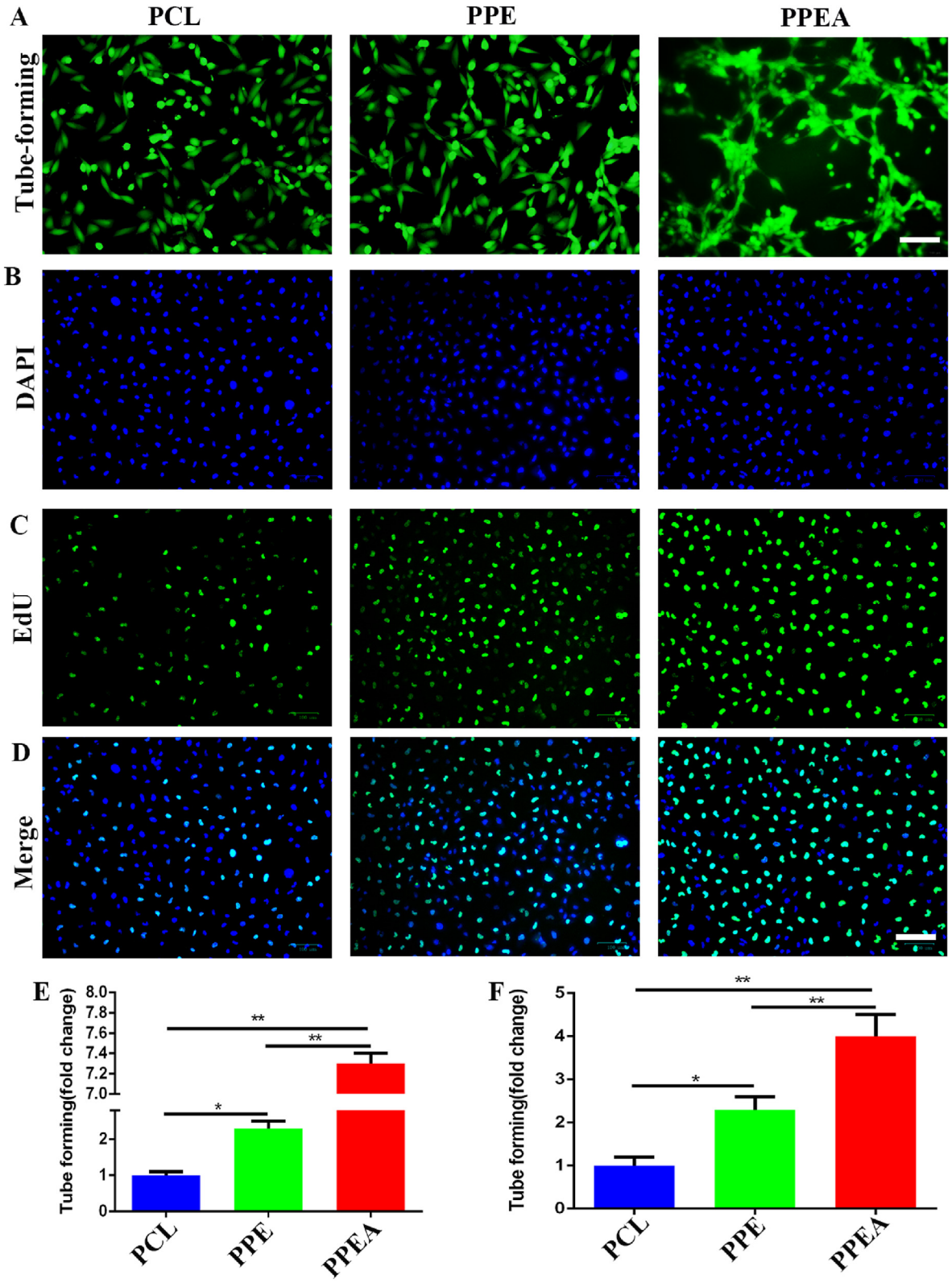

Fig. 4. PPEA biomimetic periosteum affects tubular structure and proliferation of human umbilical vein endothelial cells. (A) Tube forming experiment of biomimetic periosteum on HUVECs. (B–D) EU detected the effect of biomimetic periosteum on the proliferation of HUVECs. (E) The detection of A (F) is the detection of B-D. Scale bar = 200 μm in panels (A), Scale bar = 100 μm in panels (B–D). N = 3, *p < 0.05, **p < 0.01.

To further detect the effect of biomimetic periosteum on nerves. We first linked exosomes to PS-targeted aptamer through mPEG-COOH for composing exosomes@ aptamer (EA). As shown in (Fig. 3B), we found that PS-targeted aptamer with FAM fluorescent group was successfully loaded on exosomes through immunofluorescence.

We then cultured DRG cells and performed axonal targeting experiments. As shown in (Fig. 3C and D), EA successfully targeted the injured site of nerve axons and enriched in this area. Subsequently, we cultured

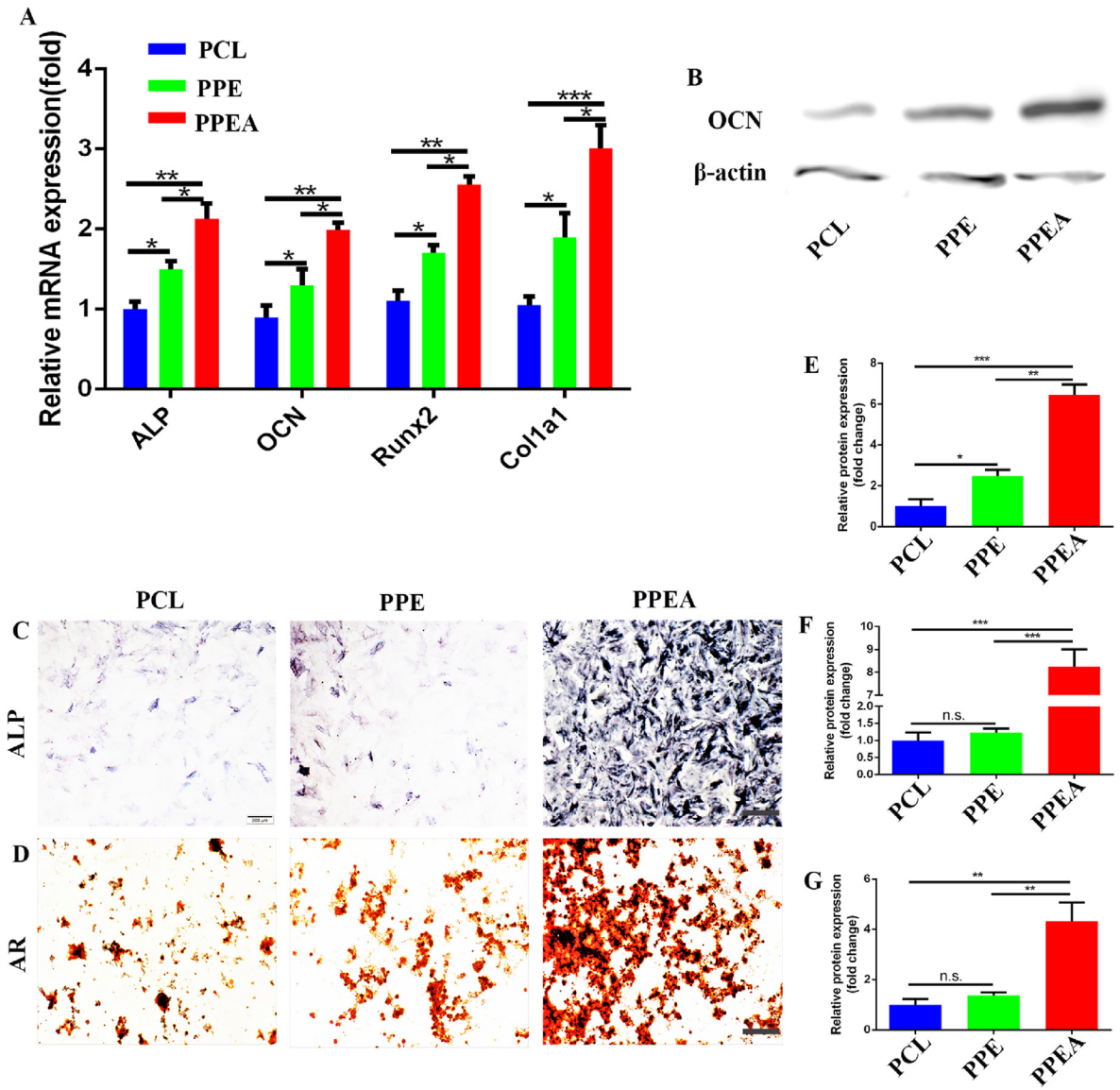

Fig. 5. Biomimetic periosteum promotes osteogenic differentiation of BMSCs. (A)RT-qPCR was used to detect the mRNA expression of ALP, OCN, Runx2, and Col1a1 in BMSCs. B Western blot was used to detect the expression of OCN protein in BMSCs. ALP (C) and AR (D) were used to detect the osteogenic transformation of BMSCs promoted by biomimetic periosteum. E-G is the quantitative analysis of B-D. Scale bar = 200 μm in panels (C, D) N = 3, *p < 0.05, **p < 0.01, ***p < 0.001.

rat dorsal root ganglion (DRG) species on the biomimetic periosteum. After two weeks, the increase in axon length in the PPEA group was more prominent (Fig. 3E–G). Compared with the control group, DRG axons showed clear guidance; axons grew in one direction (Fig. 3H–J). The above evidence proved that the PPEA biomimetic periosteum could significantly promote the regeneration and guidance of nerve axons. We also quantitatively analyzed the length of DRG axon regeneration (Fig. 3O).

Then, we detected the extracted DRG protein by Western blot. It can be seen from the figure that JNK3 in the PPEA group is significantly higher than that in the control group, which is 4.03 times that in the control group (Fig. 3K, M). We then detected JNK3 in sensory nerves by qRT PCR and immunofluorescence staining. As shown in (Fig. S6A and B), the expression of JNK3 in the nerve stimulated by EA increased significantly, which was 1.98 times that of the control group. Similarly, EA stimulation also considerably increased the expression of JNK3 mRNA, which was 8.05 times that of the control group (Fig. S6 C). This may be, after the exosome targets the injured nerve site, the exosome outer membrane combines with the nerve at the defect site to release the up-regulated JNK3 in exosomes into cells and then up-regulate the intracellular JNK3 protein. JNK3 protein is a member of the C-JUN protein family. Then we stained the vesicles of axons with FM1-43. The figure shows that the number of cysts in the PPEA group is 2.07 times that of the control group (Fig. 3L). The above evidence proves that PPEA may promote vesicle transport through the JNK MAPK pathway.

Subsequently, we detected the neuropeptide secreted by DRG. As shown in the figure, the concentration of substance P (SP) in the PPEA biomimetic periosteum group was 2.11 ng/ml, 1.82 times that of the control group (Fig. 3P, Q). And the concentration of calcitonin gene-related peptide in the PPEA biomimetic periosteum group was 27.16 pg/ml, 2.71times than that of the control group (Fig. 3I). These results showed that the PPEA biomimetic periosteum group could significantly promote the secretion of two central neuropeptides (SP and CGRP) from peripheral nerves. According to the literature, neuropeptide plays a vital role in initiating and regulating the repair of bone defects.

(A) Under different pH conditions, the release of exosomes. (B-D) EA and EA target PS in axonal damage. (E-G) Immunofluorescence was used to detect DRG axon regeneration. (H-J) The quantitative analysis of DRG axon direction. (K) The changes in the JNK3 MAPK pathway in nerve cells were detected by Western blot. (L) Changes of vesicles, (M, N)

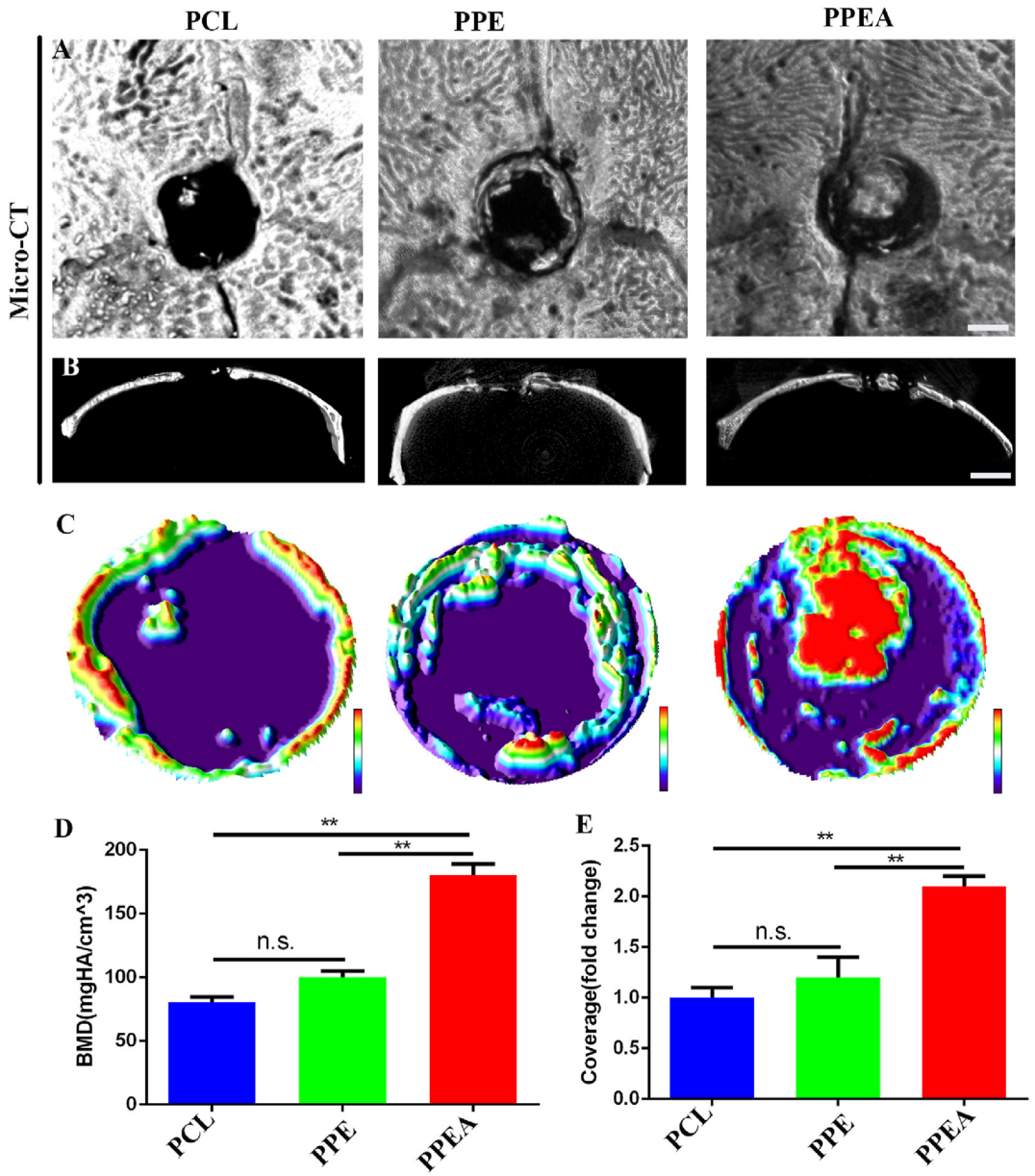

Fig. 6. Biomimetic periosteum promotes skull repair. (A) Horizontal scanning of bone defect area by micro-CT. (B) Coronal scanning of defect area by micro-CT. (C) 3D surface analysis of skull defect area. BMD analysis of new bone formation in D defect area and statistical analysis of coverage area of new bone regeneration in E defect area. Scale bar = 5 mm in panels (A, B). N = 5, **p < 0.01.

Quantification of K and L.(O) Quantification of axonal regeneration length. ELISA detection of SP (P) and CGRP (Q) in cell supernatant. Scale bar = 20 μm in panels (B, D), Scale bar = 100 μm in panels (L), Scale bar = 200 μm in panels (C, E-G). N = 3, *p < 0.05, **p < 0.01, ***p < 0.001.

3.4. Biomimetic periosteum promotes the proliferation of vascular endothelial cells and angiogenesis through DRG

Next, we added the culture medium of biomimetic periosteal culture DRG to the culture of HUVECs, and cultured HUVECs for 2 h. As shown in the figure, the tube forming effect of the PPEA biomimetic periosteum group was significantly enhanced, and the number of lines was 7.30 times that of the control group (Fig.4A, E). Subsequently, we detected the proliferation of HUVECs. As shown in the figure (Fig. 4B-D, F), the fluorescence intensity of the PPEA biomimetic periosteum group was significantly enhanced, which was 4.00 times that of the control group. The above evidence proves that neuropeptides produced by DRG cultured in PPEA biomimetic periosteum can substantially promote the proliferation and tube formation of HUVECs.

3.5. Biomimetic periosteum promotes the osteogenic transformation of MSCs through DRG

In previous reports, neuropeptide SP and CGRP have significant regulatory effects on bone regeneration [46]. Therefore, we co-cultured the culture medium of biomimetic periosteal cultured DRG with BMSCs. As shown in the figure, we first detected the mRNA expression of osteogenesis-related markers (Alkaline phosphatase (ALP), Osteocalcin (OCN), Runx2, and Col1a1). The biomimetic periosteum group showed significant up-regulation, which was 2.13, 1.99, 2.56, and 3.01 times that of the control group (Fig. 5A). Subsequently, we extracted the co-cultured proteins for detection. The figure shows that OCN was significantly up-regulated, 6.46 times more than the control (Fig. 5B, E). Finally, we used (alkaline phosphatase) ALP to detect the osteogenic effect. The

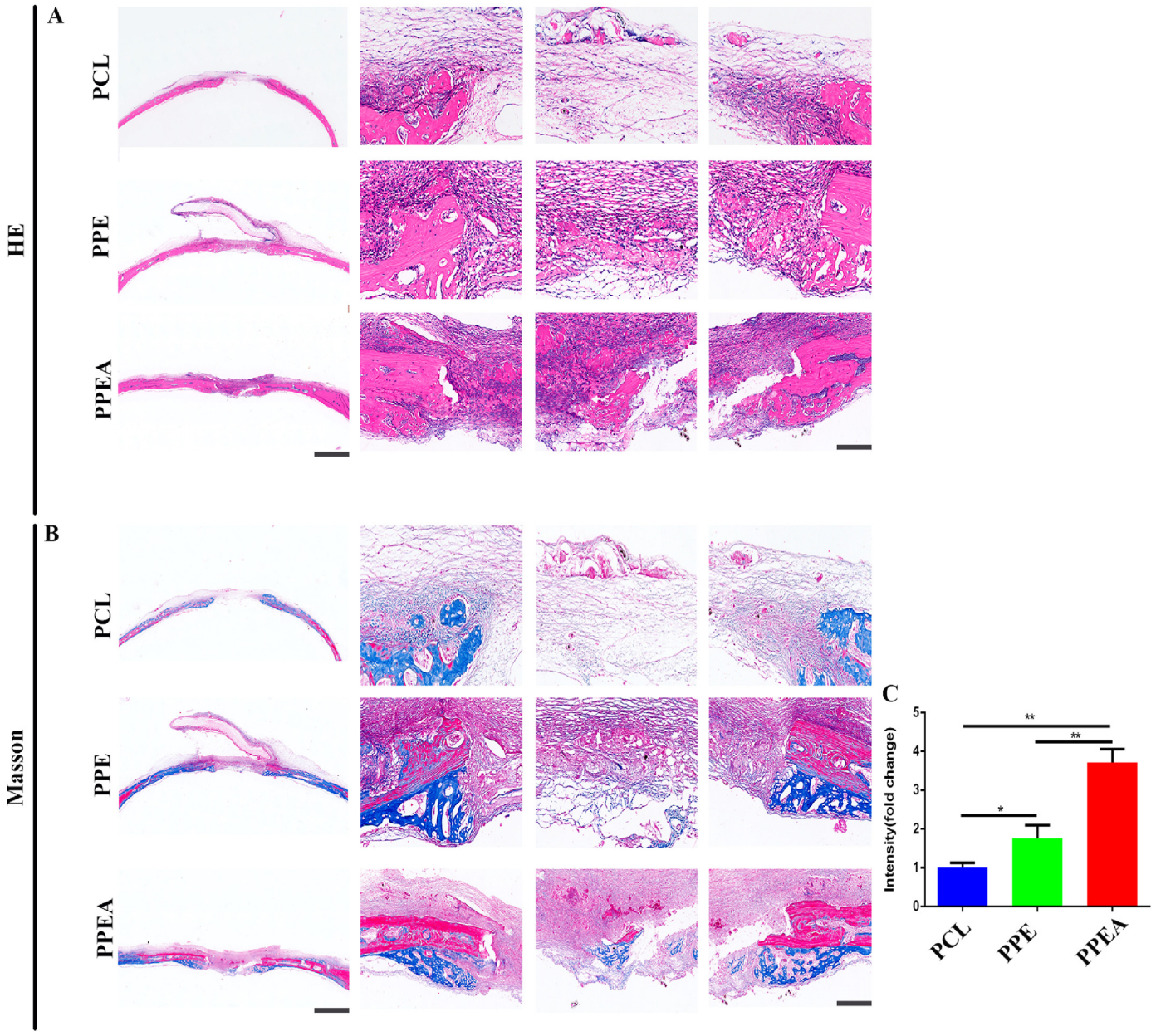

Fig. 7. Biomimetic periosteum promotes bone regeneration of skull defect. (A) HE is staining of bone defect repair by biomimetic periosteum. (B) Masson staining of bone defect repaired by biomimetic periosteum. (C) The statistical analysis of newly formed collagen in the bone defect area. Scale bar = 200 μm in whole slice, 50 μm in enlarge. N = 5, *p < 0.05, **p < 0.01.

biomimetic periosteum group had a significant promoting development, which was 8.25 times that of the control group (Fig. 5C, F). At the same time, we used alizarin red staining to detect the osteogenic effect. With the same effect, the biomimetic periosteum group showed a significant osteogenic impact, which was 4.32 times that of the control group (Fig. 5D, G). That evidence indicates that biomimetic periosteum can promote the osteogenesis of BMSCs by stimulating the secretion of neuropeptides. This PPEA biomimetic periosteum is also a further enrichment of the previously reported theory of nerve-promoting osteogenesis.

3.6. *In vivo, biomimetic periosteum promotes bone regeneration*

Subsequently, micro-CT detection shows that biomimetic periosteum can significantly promote nerve and bone regeneration in vivo; as shown in the figure, micro-CT detection shows that PPEA biomimetic periosteum can significantly promote skull repair 2.10 times more than that of the control group (Fig. 6A-C, E). BMD also increased significantly, which was 2.23 times that of the control group (Fig. 6 D). These results show that PPEA biomimetic periosteum can substantially promote the repair of bone defects in vivo.

3.7. *In vivo, biomimetic periosteum promotes collagen formation*

Collagen formation is the critical factor in bone regeneration after a bone defect [47]. Promoting collagen formation is an urgent problem in bone regeneration. Subsequently, we detected the collagen formed in the skull defect bone. As shown in the figure, the PPEA biomimetic periosteum group significantly promoted collagen formation in the skull defect area, which was 3.71 times that of the control group. The PPEA biomimetic periosteum was also higher than the PCL group, indicating that exosomes significantly promoted collagen formation (Fig. 7A–C). The

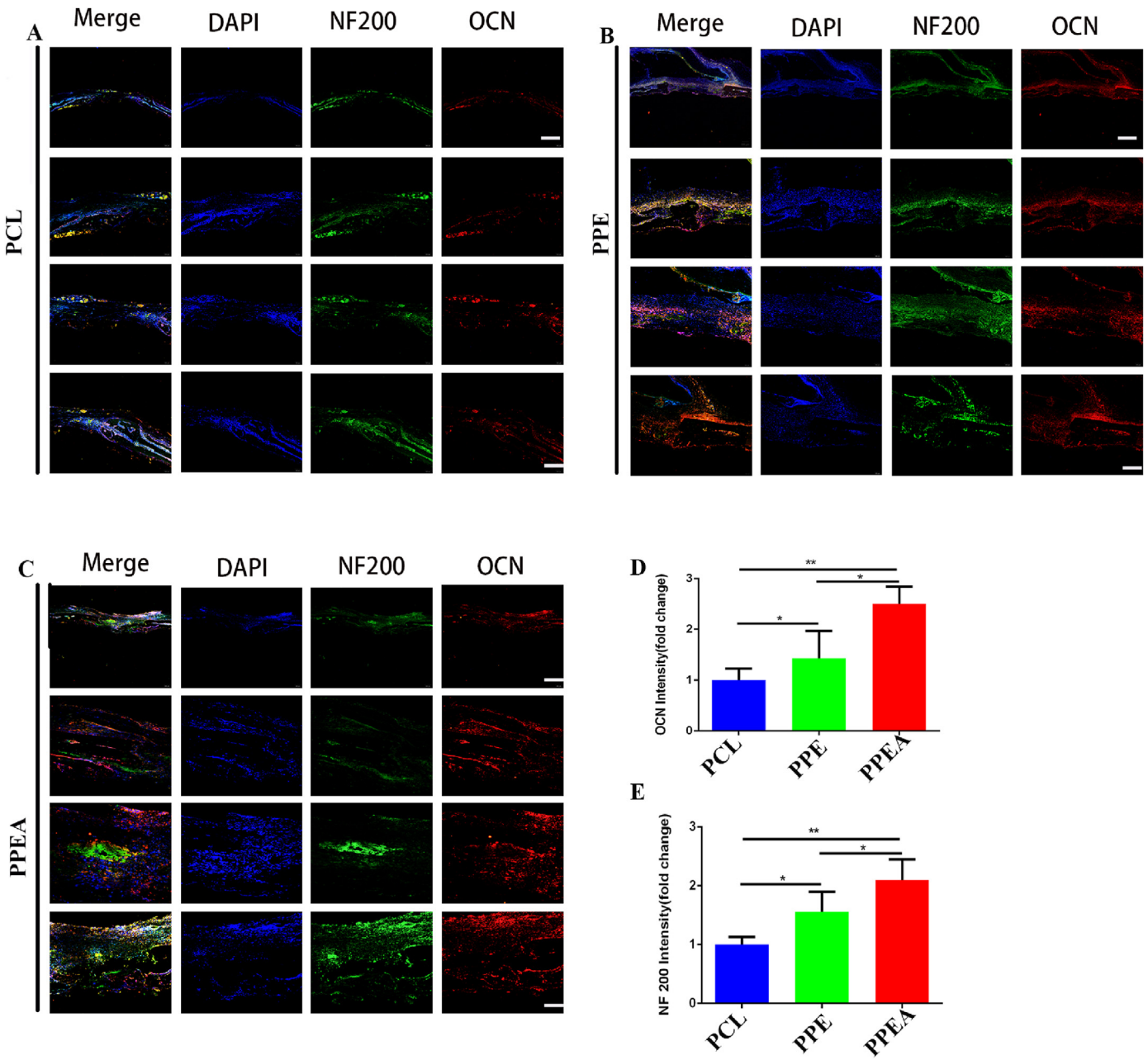

Fig. 8. Biomimetic periosteum promotes nerve regeneration and bone regeneration of bone defects. (A–C) NF200, OCN staining immunofluorescence detection of bone defect in PCL, PPE, PPEA group. (D) The quantitative analysis of nerve regeneration in A-C. (E) The quantitative analysis of bone regeneration in A-C. Scale bar = 200 μm in whole slice, 50 μm in enlarge.N = 5, *p < 0.05, **p < 0.01.

above results also confirmed that biomimetic periosteum could promote the repair of skull defects.

3.8. In vivo, the PPEA biomimetic periosteum promotes nerve regeneration and bone regeneration

Since nerve plays a crucial role in initiating and regulating bone regeneration [48], whether biomimetic periosteum can promote the formation of nerve and bone in vivo needs to be further explored. Therefore, we performed Neurofilament 200 (NF200) and OCN (osteocalcin) immunofluorescence staining on skull sections. As shown in the figure, the biomimetic periosteum group has a significant promoting effect on nerves (NF200) (Fig. 8A–C, D), which is that of the control group. At the same time, the biomimetic periosteum group also significantly promoted OCN expression, which was 2.52 times that of the control group (Fig. 8A–C, E). The above results showed that the biomimetic periosteum could significantly promote skull defects' nerve regeneration and bone regeneration.

3.9. In vivo, the PPEA biomimetic periosteum promotes angiogenesis

Subsequently, we used immunofluorescence staining of CD31 to detect the angiogenic ability of the biomimetic periosteum. As shown in Fig. 9, the number of angiogenesis in the PPEA group was the largest, which was * * times that in the PCL group.

4. Conclusions

We have successfully constructed a PPEA biomimetic periosteum and confirmed that the biomimetic periosteum could release EA in an acidic

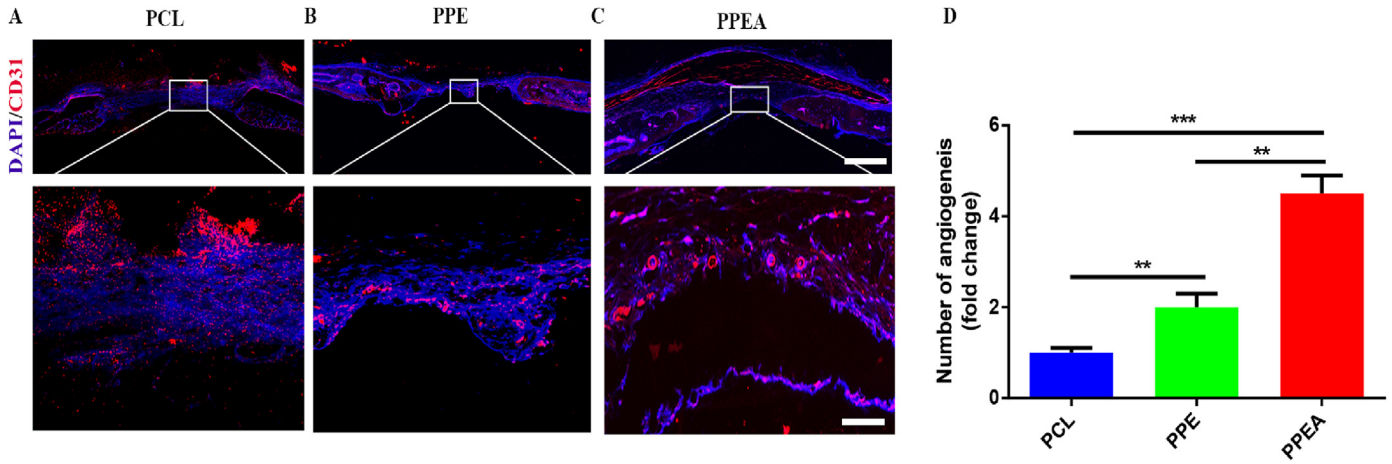

Fig. 9. Biomimetic periosteum promotes angiogenesis of bone defects. (A–C) CD31 staining immunofluorescence detection of bone defect in PCL, PPE, PPEA group. (D) The quantitative analysis of angiogenesis in A-C. Scale bar = 200 μm in whole slice, 100 μm in enlarge. N = 5, **p < 0.01, ***p < 0.001.

microenvironment and significantly induce nerve, blood vessel, and bone regeneration in vivo and in vitro experiments. Secreted EA can target injured axons, significantly promote neurovascular and bone regeneration, and provide a clear signal for remodeling the bone regeneration microenvironment. This PPEA biomimetic periosteum offers an attractive therapeutic strategy for bone regeneration and a better way for regenerative medicine by combining this active exosome with electrospinning.

Funding

This work was supported by the National Natural Science Foundation of China [grant numbers 82072446, 81873999]; the Introduction plan of high-end foreign experts of the Ministry of Science and Technology of China [grant number G2021154012L]; and the Natural Science Foundation of Hubei Province [grant number 2020BCB050].

Credit author statement

Yanlin Su, Qing Gao, Rongli Deng: conceptualization, investigation, data curation, methodology, writing-original draft preparation, writing-review&editing, formal analysis, project administration; Lian Zeng: conceptualization, data curation, methodology, writing a draft preparation; Jingyi Guo, Bing Ye: software, methodology; Jialin Yu: conceptualization, methodology, Validation, Visualization; Xiaodong Guo: conceptualization, writing-review&editing, supervision, project administration, funding acquisition. All authors have read and agreed to the published version of the manuscript.

Declaration of competing interest

The authors declare that they have no known competing financial interests or personal relationships that could have appeared to influence the work reported in this paper.

Data availability

No data was used for the research described in the article.

Acknowledgments

Thank the analysis and testing center of Huazhong University of Science and Technology for its support. Thanks to the funding support from the National Natural Science Foundation of China. The schematic diagram in each figure is created by BioRender.com and smart. We would like to thank Editage (https://www.editage.cn) for English language editing.

Appendix A. Supplementary data

Supplementary data to this article can be found online at https://doi.org/10.1016/j.mtbio.2022.100434.

References

[1] Cambre N. Kelly, Tian Wang, James Crowley, Dan Wills, Matthew H. Pelletier, Edward R. Westrick, Samuel B. Adams, Ken Gall, William R. Walsh, High-strength, porous additively manufactured implants with optimized mechanical osseointegration, Biomaterials 279 (2021), 121206, https://doi.org/10.1016/j.biomaterials.2021.121206.

[2] X.L. Sun, X.P. Li, H.Z. Qi, X. Hou, J. Zhao, X.B. Yuan, X.L. Ma, MiR-21 nanocapsules promote early bone repair of osteoporotic fractures by stimulating the osteogenic differentiation of bone marrow mesenchymal stem cells, J. Orthop. Translat. 24 (2020) 76–87, https://doi.org/10.1016/j.jot.2020.04.007.

[3] Y.S. Shi, R.J. He, X.Y. Deng, Z.W. Shao, Davide Deganello, C.Z. Yan, Z.D. Xia, Ys, Rh, Xd, Rh, Xd, Zs, Dd, Dd, Cy, Zx, Cy, Zx, Cy, Zx, Ys, Zx, Zx, Three-dimensional biofabrication of an aragonite-enriched self-hardening bone graft substitute and assessment of its osteogenicity in vitro and in vivo, Biomater. Transl. 1 (1) (2020) 69–81, https://doi.org/10.3877/cma.j.issn.2096-112X.2020.01.007.

[4] Y.Z. Peng, J.Y. Li, H. Lin, S. Tian, S. Liu, F.F. Pu, L. Zhao, K.G. Ma, X.C. Qing, Z.W. Shao, Yp, Zs, Xq, Yp, Yp, Xq, Jl, St, Yp, Xq, Jl, St, Sl, Fp, Lz, Km, Xq, Yp, Xq, Hs, St, Yp, Jl, Hl, St, Lz, Fp, Sl, Zs, Xq, Endogenous repair theory enriches construction strategies for orthopaedic biomaterials: a narrative review, Biomater. Transl. 2 (4) (2021) 343–360, https://doi.org/10.12336/biomatertransl.2021.04.008.

[5] L.J. Liu, Y. Zhang, C.J. Li, J.F. Mao, F.J. Wang, L. Wang, An enhanced periosteum structure/function dual mimicking membrane for in-situ restorations of periosteum and bone, Biofabrication 13 (3) (2021), https://doi.org/10.1088/1758-5090/abf9b0.

[6] T.S. Fu, Y.C. Wang, C.H. Chen, C.W. Chang, T.Y. Lin, C.B. Wong, D.W. Chen, C.Y. Su, Engineered periosteum-bone biomimetic bone graft enhances posterolateral spine fusion in a rabbit model, Spine J. 19 (4) (2019) 762–771, https://doi.org/10.1016/j.spinee.2018.09.013.

[7] J. Wang, J. Xu, X. Wang, L. Sheng, L. Zheng, B. Song, G. Wu, R. Zhang, H. Yao, N. Zheng, M.T. Yun Ong, P.S. Yung, L. Qin, Magnesium-pretreated periosteum for promoting bone-tendon healing after anterior cruciate ligament reconstruction, Biomaterials 268 (2021), 120576, https://doi.org/10.1016/j.biomaterials.2020.120576.

[8] Y. Li, M.D. Hoffman, D.S.W. Benoit, Matrix metalloproteinase (MMP)-degradable tissue-engineered periosteum coordinates allograft healing via early-stage recruitment and support of host neurovasculature, Biomaterials 4 (11) (2016) 1554–1561, https://doi.org/10.1016/j.biomaterials.2020.120535.

[9] R.E. Tomlinson, Z. Li, Q. Zhang, B.C. Goh, Z. Li, D.L.J. Thorek, L. Rajbhandari, T.M. Brushart, L. Minichiello, F. Zhou, A. Venkatesan, T.L. Clemens, NGF-TrkA signaling by sensory nerves coordinates the vascularization and ossification of developing endochondral bone, Cell Rep. 16 (10) (2016) 2723–2735, https://doi.org/10.1016/j.celrep.2016.08.002.

[10] B. Hu, X. Lv, H. Chen, P. Xue, B. Gao, X. Wang, G. Zhen, J.L. Crane, D. Pan, S. Liu, S. Ni, P. Wu, W. Su, X. Liu, Z. Ling, M. Yang, R. Deng, Y. Li, L. Wang, Y. Zhang, M. Wan, Z. Shao, H. Chen, W. Yuan, X. Cao, Sensory nerves regulate mesenchymal stromal cell lineage commitment by tuning sympathetic tones, J. Clin. Invest. 130 (7) (2020) 3483–3498, https://doi.org/10.1172/JCI131554.

[11] Li Ye, J. Xu, J. Mi, X. He, Q. Pan, L. Zheng, H. Zu, Z. Chen, B. Dai, X. Li, Q. Pang, L. Zou, L. Zhou, L. Huang, W. Tong, G. Li, L. Qin, Biodegradable magnesium combined with distraction osteogenesis synergistically stimulates bone tissue regeneration via CGRP-FAK-VEGF signaling axis, Biomaterials 275 (2021), 120984, https://doi.org/10.1016/j.biomaterials.2021.120984.

[12] J. Zhang, Y. Chen, Y. Huang, W. Wu, X. Deng, H. Liu, R. Li, J. Tao, X. Li, X. Liu, M. Gou, A 3D-printed self-adhesive bandage with drug release for peripheral nerve repair, Adv. Sci. (Weinh) 7 (23) (2020), 2002601, https://doi.org/10.1002/advs.202002601.

[13] Y. Zhao, Y. Liang, S. Ding, K. Zhang, H.Q. Mao, Y. Yang, Application of conductive PPy/SF composite scaffold and electrical stimulation for neural tissue engineering, Biomaterials 255 (2020), 120164, https://doi.org/10.1016/j.biomaterials.2020.120164.

[14] T. Kornfeld, J. Nessler, C. Helmer, R. Hannemann, K.H. Waldmann, C.T. Peck, P. Hoffmann, G. Brandes, P.M. Vogt, C. Radtke, Spider silk nerve graft promotes axonal regeneration on long distance nerve defect in a sheep model, Biomaterials 271 (2021), 120692, https://doi.org/10.1016/j.biomaterials.2021.120692.

[15] X. Tang, X. Gu, T. Huang, X. Chen, Z. Zhou, Y. Yang, J. Ling, Anisotropic silk-inspired nerve conduit with peptides improved the microenvironment for long-distance peripheral nerve regeneration, ACS Macro Lett. 10 (12) (2021) 1501–1509, https://doi.org/10.1021/acsmacrolett.1c00533.

[16] Y. Liu, J.R. Fang, Q. Zhang, X.G. Zhang, Y.L. Cao, W. Chen, Z.W. Shao, S.H. Yang, D.C. Wu, Man Hung, Y.Z. Zhang, W. Tong, H.T. Tian, Wnt10b-overexpressing umbilical cord mesenchymal stem cells promote critical size rat calvarial defect healing by enhanced osteogenesis and VEGF-mediated angiogenesis, J. Orthop. Translat. 23 (2020) 29–37, https://doi.org/10.1016/j.jot.2020.02.009.

[17] B. Liu, Y. Kong, W. Shi, M. Kuss, K. Liao, G. Hu, P. Xiao, J. Sankarasubramanian, C. Guda, X. Wang, Y. Lei, B. Duan, Exosomes derived from differentiated human ADMSC with the Schwann cell phenotype modulate peripheral nerve-related cellular functions, Bioact. Mater. 14 (2021) 61–75, https://doi.org/10.1016/j.bioactmat.2021.11.022.

[18] S.M. Gysler, R. Drapkin, Tumor innervation: peripheral nerves take control of the tumor microenvironment, J. Clin. Invest. 131 (11) (2021), e147276, https://doi.org/10.1172/JCI147276.

[19] A. Hervera, F. De Virgiliis, I. Palmisano, L. Zhou, E. Tantardini, G. Kong, T. Hutson, M.C. Danzi, R.B. Perry, C.X.C. Santos, A.N. Kapustin, R.A. Fleck, J.A. Del Río, T. Carroll, V. Lemmon, J.L. Bixby, A.M. Shah, M. Fainzilber, S. Di Giovanni, Reactive oxygen species regulate axonal regeneration through the release of exosomal NADPH oxidase 2 complexes into injured axons, Nat. Cell Biol. 20 (3) (2018) 307–319, https://doi.org/10.1038/s41556-018-0039-x.

[20] T.T. Yu, Y.X. Xu, Muhammad Arslan Ahmad, Rabia Javed, Haruo Hagiwara, X.H. Tian, Exosomes as a promising therapeutic strategy for peripheral nerve injury, Curr. Neuropharmacol. 19 (12) (2021) 2141–2151, https://doi.org/10.2174/1570159X19666210203161559.

[21] P.J. Arthur-Farraj, C.C. Morgan, M. Adamowicz, J.A. Gomez-Sanchez, S.V. Fazal, A. Beucher, B. Razzaghi, R. Mirsky, K.R. Jessen, T.J. Aitman, Changes in the coding and non-coding transcriptome and DNA methylome that define the Schwann cell repair phenotype after nerve injury, Cell Rep. 20 (11) (2017) 2719–2734, https://doi.org/10.1016/j.celrep.2017.08.064.

[22] K.R. Jessen, P. Arthur-Farraj, Repair Schwann cell update: adaptive reprogramming, EMT, and stemness in regenerating nerves, Glia 67 (3) (2019) 421–437, https://doi.org/10.1002/glia.23532.

[23] Hannah Faris, Mohammadali Almasieh, Leonard A. Levin, Axonal degeneration induces distinct patterns of phosphatidylserine and phosphatidylethanolamine externalization, Cell Death Dis. 7 (1) (2021) 247, https://doi.org/10.1038/s41420-021-00641-7.

[24] Brent Neumann, Sean Coakley, Rosina Giordano-Santini, Casey Linton, Eui Seung Lee, Akihisa Nakagawa, Xue Ding, Massimo A. Hilliard, EFF-1-mediated regenerative axonal fusion requires components of the apoptotic pathway, Nature 517 (7533) (2015) 219–222, https://doi.org/10.1038/nature14102.

[25] Md Ashrafuzzaman, Chih-Yuan Tseng, Janice Kapty, John R. Mercer, Jack A. Tuszynski, A computationally designed DNA aptamer template with specific binding to phosphatidylserine, Nucleic Acid Therapeut. 23 (6) (2013) 418–426, https://doi.org/10.1089/nat.2013.0415.

[26] S. Vedaraman, A. Perez-Tirado, T. Haraszti, J. Gerardo-Nava, A. Nishiguchi, L. De Laporte, Anisometric microstructures to determine minimal critical physical cues required for neurite alignment, Adv. Healthc. Mater. 10 (20) (2021), e2100874, https://doi.org/10.1002/adhm.202100874.

[27] G. Li, C. Xue, H. Wang, X. Yang, Y. Zhao, L. Zhang, Y. Yang, Spatially featured porous chitosan conduits with micropatterned inner wall and seamless sidewall for bridging peripheral nerve regeneration, Carbohydr. Polym. 194 (2018) 225–235, https://doi.org/10.1016/j.carbpol.2018.04.049.

[28] L. Huang, J. Gao, H. Wang, B. Xia, Y. Yang, F. Xu, X. Zheng, J. Huang, Z. Luo, Fabrication of 3D scaffolds displaying biochemical gradients along longitudinally oriented microchannels for neural tissue engineering, ACS Appl. Mater. Interfaces 12 (43) (2020) 48380–48394, https://doi.org/10.1021/acsami.0c15185.

[29] F. Milos, G. Tullii, F. Gobbo, F. Lodola, F. Galeotti, C. Verpelli, D. Mayer, V. Maybeck, A. Offenhäusser, M.R. Antognazza, High aspect ratio and light-sensitive micropillars based on a semiconducting polymer optically regulate neuronal growth, ACS Appl. Mater. Interfaces 13 (20) (2021) 23438–23451, https://doi.org/10.1021/acsami.1c03537.

[30] D. Zhang, S. Wu, J. Feng, Y. Duan, D. Xing, C. Gao, Micropatterned biodegradable polyesters clicked with CQAASIKVAV promote cell alignment, directional migration, and neurite outgrowth, Acta Biomater. 74 (2018) 143–155, https://doi.org/10.1016/j.actbio.2018.05.018.

[31] Z.L. Rao, T. Lin, S. Qiu, J. Zhou, S. Liu, S.H. Chen, T. Wang, X.L. Liu, Q.T. Zhu, Y. Bai, D.P. Quan, Decellularized nerve matrix hydrogel scaffolds with longitudinally oriented and size-tunable microchannels for peripheral nerve regeneration, Mater. Sci. Eng. C Mater. Biol. Appl. 120 (2021), 111791, https://doi.org/10.1016/j.msec.2020.111791.

[32] Ben Kaplan, Shulamit Levenberg, The role of biomaterials in peripheral nerve and spinal cord injury: a review, Int. J. Mol. Sci. 23 (3) (2022) 1244, https://doi.org/10.3390/ijms23031244.

[33] X.J. Yang, Y.T. Wang, Y. Zhou, J.Y. Chen, Q.B. Wan, The application of polycaprolactone in three-dimensional printing scaffolds for bone tissue engineering, Polymers (Basel) 13 (16) (2021) 2754, https://doi.org/10.3390/polym13162754.

[34] Y.H. Hou, W.G. Wang, Paulo Bartolo, Investigation of polycaprolactone for bone tissue engineering scaffolds: in vitro degradation and biological studies, Mater. Des. (2022), 110582, https://doi.org/10.1016/j.matdes.2022.110582.

[35] Y. Xu, J. Zhao, Z. Zhang, J. Zhang, M. Huang, S. Wang, P. Xie, Preparation of electrospray ALG/PDA-PVP nanocomposites and their application in cancer therapy, Soft Matter 16 (1) (2020) 132–141, https://doi.org/10.1039/c9sm01584a.

[36] M.P. Arrieta, A. Leonés Gil, M. Yusef, J.M. Kenny, L. Peponi, Electrospinning of PCL-based blends: processing optimization for their scalable production, Materials (Basel) 13 (17) (2020) 3853, https://doi.org/10.3390/ma13173853.

[37] T.F. Sun, M. Liu, S. Yao, Y.H. Ji, Z.K. Xiong, K. Tang, K.F. Chen, H. Yang, X.D. Guo, Biomimetic composite scaffold containing small intestinal submucosa and mesoporous bioactive glass exhibits high osteogenic and angiogenic capacity, Tissue Eng. 24 (13–14) (2018) 1044–1056, https://doi.org/10.1089/ten.TEA.2017.0398.

[38] K.R. Jessen, R. Mirsky, The repair Schwann cell and its function in regenerating nerves, J. Physiol. 594 (13) (2016) 3521–3531, https://doi.org/10.1113/JP270874.

[39] David B. Parkinson, Ziping Dong, Bunting Howard, Jonathan Whitfield, Carola Meier, Hélène Marie, Rhona Mirsky, R. Kristjan, Jessen, Transforming growth factor β (TGFβ) mediates Schwann cell death in vitro and in vivo: examination of c-jun activation, interactions with survival signals, and the relationship of TGFβ-mediated death to Schwann cell differentiation, J. Neurosci. 21 (21) (2001) 8572–8585, https://doi.org/10.1523/JNEUROSCI.21-21-08572.2001.

[40] R. Bahulekar, N.R. Ayyangar, S. Ponrathnam, Polyethyleneimine in immobilization of biocatalysts, Enzym. Microb. Technol. 13 (11) (1991) 858–868, https://doi.org/10.1016/0141-0229(91)90101-f.

[41] Pol Escudé Martinez de Castilla, L.J. Tong, C.Y. Huang, Alexandros Marios Sofia, Giorgia Pastorin, X.Y. Chen, Gert Storm, Raymond M. Schiffelers, J.W. Wang, Extracellular vesicles as a drug delivery system: a systematic review of preclinical studies, Adv. Drug Deliv. Rev. 175 (2021), 113801, https://doi.org/10.1016/j.addr.2021.05.011.

[42] Y.L. Zhang, D.J. Chen, B.L. Yang, T.T. Liu, J.J. Li, X.Q. Wang, G.Y. Xue, Z.X. Liu, Microencapsulated Schwann cell transplantation inhibits P2X3 receptor expression in dorsal root ganglia and neuropathic pain, Neural Regen. Res. 13 (11) (2018) 1961–1967, https://doi.org/10.4103/1673-5374.238715.

[43] Vig Sanjana, Maria Helena Fernandes, Bone cell exosomes and emerging strategies in bone engineering, Biomedicines 10 (4) (2022) 767, https://doi.org/10.3390/biomedicines10040767.

[44] R. Bahulekar, N.R. Ayyangar, S. Ponrathnam, Polyethyleneimine in immobilization of biocatalysts, Enzym. Microb. Technol. 13 (11) (1991) 858–868, https://doi.org/10.1016/0141-0229(91)90101-f.

[45] Julia C. Berkmann, Aaron X Herrera Martin, Agnes Ellinghaus, Claudia Schlundt, Schell Hanna, Evi Lippens, Georg N. Duda, Serafeim Tsitsilonis, Katharina Schmidt-Bleek, Early pH changes in musculoskeletal tissues upon injury-aerobic catabolic pathway activity linked to inter-individual differences in local pH, Int. J. Mol. Sci. 21 (7) (2020) 2513, https://doi.org/10.3390/ijms21072513.

[46] S. Sun, N.H. Diggins, Z.J. Gunderson, J.C. Fehrenbacher, F.A. White, M.A. Kacena, No pain, no gain? The effects of pain-promoting neuropeptides and neurotrophins on fracture healing, Bone 131 (2020), 115109, https://doi.org/10.1016/j.bone.2019.115109.

[47] D.W. Zhang, X.W. Wu, J.D. Chen, K.L. Lin, The development of collagen-based composite scaffolds for bone regeneration, Bioact. Mater. 3 (1) (2018) 129–138, https://doi.org/10.1016/j.bioactmat.2017.08.004.

[48] Alessandra Marrella, Tae Yong Lee, Dong Hoon Lee, Sobha Karuthedom, Denata Syla, Aditya Chawla, Khademhosseini Ali, Hae Lin Jang, Engineering vascularized and innervated bone biomaterials for improved skeletal tissue regeneration, Mater. Today (Kidlington) 21 (4) (2018) 362–376, https://doi.org/10.1016/j.mattod.2017.10.005.